

Bayesian method for quantifying the non-Gaussian fluctuations in low-intermediate energy heavy ion collisions

Xinyu Wang^a, Xiang Chen^a, Junping Yang^a, Ying Cui^{a,*}, Zhuxia Li^a, Kai Zhao^{a,*}, Yingxun Zhang^{a,b,c,*}

^aChina Institute of Atomic Energy P. O. Box 275(18) Beijing 102413 China

^bDepartment of Physics and Technology Guangxi normal University Guilin 540101 China

^cShanghai Research Center for Theoretical Nuclear Physics NSFC and Fudan University Shanghai 200438 China

Abstract

In this work, we present a model-independent method to quantify the non-Gaussian fluctuations in the observable distributions, which are assessed by the difference between the measured observable distributions and reconstructed observable distributions via the Bayesian method. Our results indicate that the strength of non-Gaussian fluctuation increases with the beam energy, and is primarily driven by non-central collision mechanisms. The experimental measurement of the strength of non-Gaussian fluctuation of the observable distributions will provide valuable insights into understanding the nonequilibrium effects in heavy ion collisions and the liquid-gas phase transition in finite nuclei.

Keywords: Bayesian method, non-Gaussian fluctuations, impact parameter distributions, observable distributions

The Bayesian method is a statistical approach that involves using probability to represent uncertainty in the knowledge about model parameters and is widely used in algorithms of statistical analysis and machine learning[1]. For example, the Bayesian inference on the nuclear equation of state[2; 3; 4; 5], a Bayesian Neural Network for approximating the nuclear fission yield data and nuclear mass[6; 7; 8], a Naive Bayes Classifier for predicting nuclear charge radii and mass[9; 10], Richard-Lucy algorithm for deblurring and accurately identifying sources[11]. Recently, the Bayesian method for reconstructing the impact parameter distributions and understanding the fluctuation mechanism for intermediate and high energy heavy ion collisions (HICs) were performed[12; 13; 14; 15].

In Ref.[16], Chen et al. extended this Bayesian method to low-intermediate energy HICs for reconstructing the impact parameter distribution with two observables, such as the multiplicity of charged particles M and total transverse momentum of light charged particles, p_t^{tot} . In this extension, the fluctuation kernel of observable with respect to the impact parameter was assumed as a two-dimensional Gaussian form, and the reconstruction of the impact parameter was achieved. This advancement allows for a more comprehensive understanding not only on the impact parameter distributions but also on the associated non-Gaussian fluctuation in the observable distribution in low-intermediate energy HICs.

More details, the strength of the non-Gaussian fluctuation is measured by the deviations between the measured and reconstructed observable distribution since the reconstructed observable distribution is built from the Gaussian fluctuation kernel.

Theoretically, the deviation can be attributed to the memory effects of the nonequilibrium dynamical process[17] or the large correlation length near the critical point [18; 19; 20; 21; 22; 23]. As the phenomena associated with the critical point are universal, such as the proliferation of fluctuations, one can also expect that the non-Gaussian fluctuation may appear for nuclear liquid-gas phase transition.

To deeply understand the origins of the fluctuation of observable, i.e., the observable distribution, a comprehensive investigation was conducted within the framework of the improved quantum molecular dynamics model (ImQMD)[24; 25] in Ref.[16]. Their results evidence that the initial states of the simulated events have a Gaussian fluctuation nature, which arises from the stochastic sampling of nucleon positions and momenta[26; 25; 27]. While the nucleonic potential and nucleon-nucleon collisions, which dominate the mechanism of the fragmentation and the mechanism of the liquid-gas phase transition, have the potential to distort the Gaussian fluctuation. Thus, quantitatively analyzing the non-Gaussian fluctuation of the HICs data is essential for us to understand the liquid-gas phase transition in nuclear matter and develop an advanced microscopic transport model.

In this work, a model-independent method for quantifying the strength of non-Gaussian fluctuations in observables is proposed and its strength is investigated with respect to impact parameter b and beam energy E_{beam} under two different effective nucleon-nucleon interactions. The paper is organized as follows. Firstly, we generate the ‘measured’ observable distributions with the ImQMD model and filter them with the experimental conditions. Then, the reconstruction of the impact parameter distribution and observable distributions via the Bayesian method are investigated under the experimental conditions. By comparing the reconstructed observable distribu-

*Corresponding author

Email addresses: yingcuid@163.com (Ying Cui), zhaokai@ciae.ac.cn (Kai Zhao), zhyx@ciae.ac.cn (Yingxun Zhang)

tions with ‘measured’ observable distributions, we quantify the deviation between them by using the mean-square-error (MSE). This MSE value also serves as the indicator of the strength of non-Gaussian fluctuations. Our theoretical results show MSE increases with the beam energy due to the strong nonequilibrium effect of the mid-peripheral collisions.

The ‘measured’ observables in this study are the multiplicity of charged particles, i.e., M , and the total transverse momentum of light charged particles, i.e., p_t^{tot} , for reaction system $^{112}\text{Sn}+^{112}\text{Sn}$ at the beam energies ranging from 50 MeV/u to 200 MeV/u. These data are generated using the ImQMD model(the ImQMD-Sky version)[24]. The impact parameter b is randomly distributed within the range from 0 to $b_{max} = 1.2(A_p^{1/3} + A_t^{1/3})$ fm according to the probability density $2b/b_{max}^2$, and the total events number is 1,000,000. A_p and A_t are the mass numbers of projectile and target, respectively. The effective Skyrme interaction SkM* and SLy4 are used in the calculations. More details of this model can be found in Refs.[24; 25; 27].

To elucidate the impacts of the experimental filters, we use the angle and energy cuts as in Ref.[28], i.e., θ_{lab} from 14° to 80° and 100° to 147° , where θ_{lab} is the angle in laboratory reference frame, and the emitted particles with kinetic energy ranging from 10 MeV to 100 MeV are detected. A sketch plot of the detectors is presented in Fig. 1. The reason why we use the transport model to generate the ‘measured’ data is that we know the impact parameter b , p_t^{tot} , and M for each event. This allows us to check the effectiveness of the Bayesian method on the reconstruction of impact parameter distributions and the form observable distributions at different b .

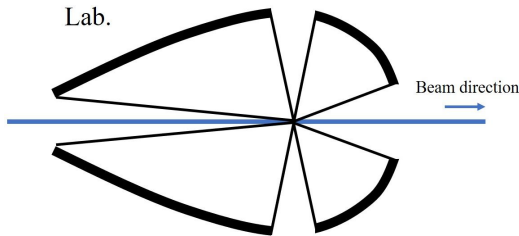


Figure 1: Schematic representation of the experimental detector setup.

Now, let us first introduce the Bayesian method for model-independently reconstructing impact parameter distributions[12; 14; 15; 16]. This method is based on Bayes’s theorem,

$$P(b|\mathbf{X}) = \frac{P(b)P(\mathbf{X}|b)}{P(\mathbf{X})}. \quad (1)$$

Here, $P(\mathbf{X})$ represents the probability density of the observable \mathbf{X} over the whole impact parameter, which can be measured in experiments. The $P(\mathbf{X}|b)$ denotes the conditional probability density distribution of $\mathbf{X} = (M, p_t^{tot})$ at a given impact parameter b , and is also named as the fluctuation kernel. By utilizing Eq.(1), one can infer the impact parameter distribution at specific values of \mathbf{X} , i.e., $P(b|\mathbf{X})$, if the probability density functions (PDFs) $P(b)$ and $P(\mathbf{X}|b)$ are known.

To avoid the uncertainties from the $P(b)$, the b -centrality (c_b)

is introduced as the same as in [12],

$$c_b = \int_0^b P(b')db'. \quad (2)$$

This allows for the replacement of the variable b , resulting in $P(c_b) = 1$. Thus, a simple form, i.e.,

$$P(\mathbf{X}) = \int P(\mathbf{X}|c_b)dc_b, \quad (3)$$

can be obtained. By fitting the data of $P(\mathbf{X})$, one can obtain the solution for $P(\mathbf{X}|c_b)$ if the form of $P(\mathbf{X}|c_b)$ is given¹.

In this study, the form of $P(\mathbf{X}|c_b)$ is assumed as a Gaussian distribution as same as in Refs.[15; 16] and we renamed it as,

$$P_G(\mathbf{X}|c_b) = \frac{\exp\{-\frac{1}{2}(\mathbf{X} - \bar{\mathbf{X}}(c_b))^T \Sigma^{-1}(c_b)(\mathbf{X} - \bar{\mathbf{X}}(c_b))\}}{2\pi \sqrt{|\Sigma(c_b)|}}. \quad (4)$$

The mean values $\bar{\mathbf{X}}$ and the elements of the covariance matrix Σ_{ij} are smooth positive functions of c_b , and are expressed as the exponential of a polynomial as in Ref. [15],

$$\begin{aligned} \bar{X}_i(c_b) &= \bar{X}_i(0) \exp\left(-\sum_{n=1}^{n_{max}} a_{i,n} c_b^n\right), \quad i = 1, \dots, N, \\ \Sigma_{ij}(c_b) &= \Sigma_{ij}(0) \exp\left(-\sum_{m=1}^{m_{max}} A_{ij,m} c_b^m\right), \quad i = 1, \dots, N. \end{aligned} \quad (5)$$

We rename the reconstructed observable distributions as $Q(\mathbf{X})$, which is,

$$Q(\mathbf{X}) = \int P_G(\mathbf{X}|c_b)dc_b. \quad (6)$$

The values of n_{max} , m_{max} , $\bar{X}_i(0)$, $a_{i,n}$, $\Sigma_{ij}(0)$ and $A_{ij,m}$ of $P_G(\mathbf{X}|c_b)$ are determined by describing the ‘measured’ data of $P(\mathbf{X})$ with a minimum of the reduced chi-square, i.e., $\chi_r^2 \geq \chi_{r,min}^2$. More details, the values of M and p_t^{tot} are rescaled by their maximum values to make their values less than 1, i.e., $M_0 = M/M_{max}$ and $p_{t0}^{tot} = p_t^{tot}/p_{t,max}^{tot}$, for constructing the $\mathbf{X} = \{M_0, p_{t0}^{tot}\}$ as a dimensionless vector in the Bayesian analysis of multiobservables. The values of M_{max} and $p_{t,max}^{tot}$ obtained with SkM* and different beam energies are listed in the second and third columns of Table 1. The normalization procedure does not influence our conclusions as evidenced in Ref.[16].

Table 1: The maximum multiplicity of charged particles and the total transverse momentum of light charged particles under the experimental filter for the $^{112}\text{Sn}+^{112}\text{Sn}$ at 50 MeV/u and 120 MeV/u. E_{beam} is in MeV/u, and $p_{t,max}^{tot}$ is in GeV/c. The last six columns are reduced $\chi_{r,n_{max}m_{max}}^2$ obtained by reconstruction method with different combinations of n_{max} and m_{max} .

E_{beam}	M_{max}	$p_{t,max}^{tot}$	$\chi_{r,11}^2$	$\chi_{r,22}^2$	$\chi_{r,23}^2$	$\chi_{r,32}^2$	$\chi_{r,33}^2$	$\chi_{r,44}^2$
50	45	13	1.53	1.21	1.16	1.13	1.10	1.06
120	62	24	8.49	2.09	1.60	2.20	2.15	4.55

The color maps in Figure. 2 present the $P(\mathbf{X})$ s for $^{112}\text{Sn}+^{112}\text{Sn}$, which are generated directly from the ImQMD

¹which is equal of $P(\mathbf{X}|b)$

with SkM* parameter set and serve as the ‘measured’ data. Panel (a) and (b) are the results for the beam energy at 50 MeV/u and 120 MeV/u, respectively. At 120 MeV/u, the largest value of $P(\mathbf{X})$ appears at small M_0 and p_{t0}^{tot} region which corresponds to peripheral collision events. With the beam energy decreasing to 50 MeV/u, the reaction system enters into the spinodal region, where the tiny fluctuation of the system states will dramatically change the final fragmentation pattern. These different fragmentation patterns lead to the strong fluctuation of observables relative to the b , and thus the $P(\mathbf{X})$ have a flat distribution over a wide range of M_0 and p_{t0}^{tot} .

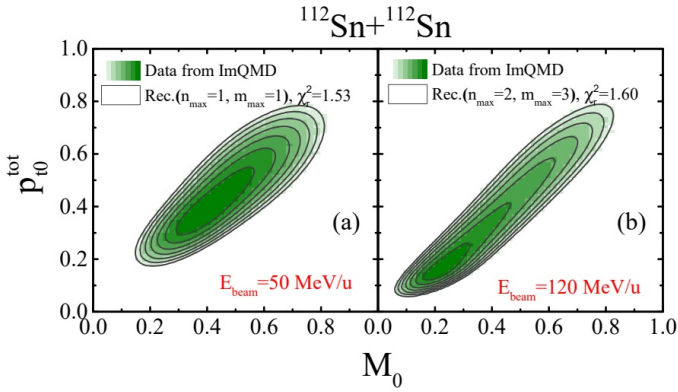


Figure 2: Contour plots of probability density distribution M_0 vs p_{t0}^{tot} for $^{112}\text{Sn}+^{112}\text{Sn}$ at $E_{beam}=50$ MeV/u (a) and 120 MeV/u (b). The lines are the reconstructed results.

The contour lines in Fig. 2 are the reconstructed results, i.e., $Q(\mathbf{X})$, obtained with the smallest number of n_{max} and m_{max} combinations and smallest χ_r^2 value among the different n_{max} and m_{max} combinations. This reconstruction depends on the solution of the $P_G(\mathbf{X}|c_b)$, which requires to determine the 6 groups of parameters in Eq.(5), such as $\bar{X}_i(0)$, $a_{i,n}$, $\Sigma_{ij}(0)$, $A_{ij,m}$, n_{max} , and m_{max} . The index i ranges from 1 to N , n from 1 to n_{max} , and m from 1 to m_{max} . Thus, the total number of parameters N_{para} is,

$$N_{para} = N(n_{max} + 1) + \frac{N(N + 1)}{2}(m_{max} + 1). \quad (7)$$

In this work, $N = 2$. n_{max} and m_{max} can take different combinations. When $n_{max} = 1$ and $m_{max} = 1$, $N_{para} = 10$ and when $n_{max} = 4$ and $m_{max} = 4$, $N_{para} = 25$. These parameters are determined by fitting the ‘measured’ data $P(\mathbf{X})$ with the MINUIT[29].

However, one should keep in mind that it is hard to justify how many fitting parameters are good enough by only seeking the minimum of χ_r^2 among the different parameter sets, since the real b dependence of \bar{X}_i and Σ_{ij} or the real b distribution are not known in advance in experiments. Thus, we also list the values of χ_r^2 obtained with other combinations of n_{max} and m_{max} in Table 1 which will be used to estimate the uncertainties of the reconstructed method.

In Fig.3, we plot the predicted reduced impact parameter $b_0 = b/b_{max}$ distributions (shaded regions), i.e., $P(b_0|\mathbf{X})$, by

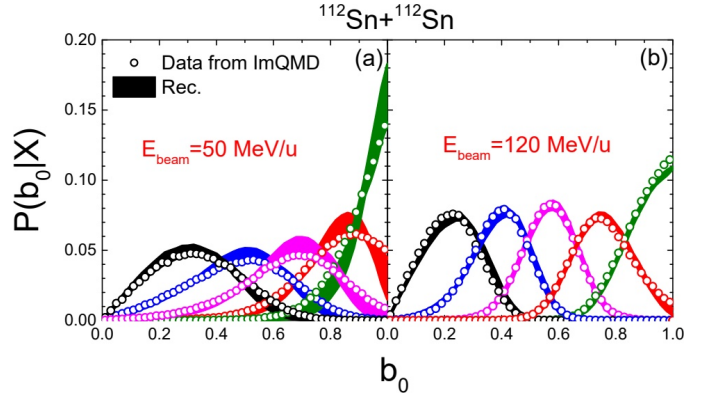


Figure 3: Reduced impact parameter distributions for five clusters; open circles are the impact parameter distributions obtained from ImQMD model with SkM*, and shaded regions are the results inferred with the reconstructing method with different n_{max} and m_{max} combinations.

using the Bayesian method, i.e.,

$$P(b|\mathbf{X} \in C_k) = P(b)P(c_b|\mathbf{X} \in C_k) = \frac{P(b) \int_{\mathbf{X} \in \Omega(C_k)} P_G(\mathbf{X}|c_b) d\mathbf{X}}{\int_{\mathbf{X} \in \Omega(C_k)} P(\mathbf{X}) d\mathbf{X}}. \quad (8)$$

C_k is the subset of the i th classification of data \mathbf{X} by using the K -means method as same as in Ref.[16]. The shaded bands in the figure are the results obtained with $\chi_r^2 < \chi_{r,min}^2 + 1$ for different combination of n_{max} and m_{max} . As detailed in Table 1, all the values of $\chi_{r,n_{max}m_{max}}^2$ obtained with our selected combinations are less than $\chi_{r,min}^2 + 1$ for $E_{beam}=50$ MeV/u. For $E_{beam} = 120$ MeV/u, there are four combinations of n_{max} and m_{max} that yield the $\chi_{r,n_{max}m_{max}}^2 < \chi_{r,min}^2 + 1$. It indicates larger uncertainties of n_{max} and m_{max} for $E_{beam} = 50$ MeV/u than that for $E_{beam} = 120$ MeV/u, and result in a wider uncertainty region of the reconstructed impact parameter distributions as in panel (a) than that in panel (b). Nonetheless, the figure illustrated that the predicted reduced impact parameter distributions from the reconstructing method agree well with the actual impact parameter distributions (open circles) under the different combinations of n_{max} and m_{max} . The high fidelity of the reconstructed impact parameter distributions allows us to understand the strength of the non-Gaussian fluctuation as a function of impact parameter or centrality in experiments.

In general, the fluctuations of observables with respect to b stem from the addition of the random sources of the initialization and nucleon-nucleon scattering on smaller scales[16]. The assumption on the Gaussian form of $P(\mathbf{X}|c_b)$ implies that the systems reach equilibrium since the observables from different events and different impact parameters are independent of each other. Thus, the deviation between $P(\mathbf{X})$ and $Q(\mathbf{X})$ quantifies the strength of non-Gaussian fluctuation, and can reflect the nonequilibrium effect of heavy ion collisions. Nonetheless, the obtained χ_r^2 can not completely measure the deviation between $P(\mathbf{X})$ and $Q(\mathbf{X})$. The reason is that the χ_r^2 is obtained only within the ‘measured’ data region, i.e., the region with $P(\mathbf{X}) \neq 0$, and does not consider the difference of two distributions in the region where $P(\mathbf{X}) = 0$ but $Q(\mathbf{X}) \neq 0$.

Usually, the cumulants of the observable are used to quantify the non-Gaussian fluctuations in the field of high energy HICs for investigating the phase transition [30; 31; 32]. However, the relation between different cumulants becomes much more complicated for two observables than only using one observable. Thus, we use the mean-square-error (MSE), which is defined as,

$$\text{MSE}(P||Q) = \frac{1}{S} \sum_{i=1}^S (P(\mathbf{X}_i) - Q(\mathbf{X}_i))^2, \quad (9)$$

to quantify the strength of the non-Gaussian fluctuations. $P(\mathbf{X}_i)$ and $Q(\mathbf{X}_i)$ in Eq.(9) represent the ‘measured’ and reconstructed probability density distribution for \mathbf{X} at mesh point i ($i = 1, \dots, S$) in a unitary area, respectively. S is the number of the mesh points in the whole area. The factor $1/S$ is used to normalize the result.

Fig.4 (a) shows the MSE as a function of beam energy within the range of 200 MeV per nucleon (red and blue stars). Generally, the values of MSE increase with beam energy for two kinds of effective interactions, which is caused by the decreasing of the equilibrium degree of the system as the beam energy increases. To deep understand it, we also analyze the MSE as a function of E_{beam} at $b=1, 6, 8,$ and 10 fm, which are calculated by using Eq.(9) but the $P(\mathbf{X}_i)$ and $Q(\mathbf{X}_i)$ are replaced by the conditional probabilities $P(\mathbf{X}_i|b)$ and $P_G(\mathbf{X}_i|b)$ at given b . As illustrated in the figure, the MSE weakly increases with the b increasing from central collisions to peripheral collisions at the beam energy less than 120 MeV/u. This increasing trend is caused by the growing anisotropy with impact parameter increasing in the overlapped region, which makes the emitted particles carry more entrance channel information. Thus, their distributions tend to deviate from the Gaussian shape, and the values of MSE become larger than those for central collisions due to the stronger nonequilibrium effect. With the beam energy increasing above 120 MeV/u, the b dependence of MSE becomes stronger since the nonequilibrium effect becomes more strong, especially for $b > 6$ fm.

However, the impact parameter weight is taken into account in the calculations of MSE at different b in panel (a), which may lead a misunderstanding on the strength of non-Gaussian fluctuation at different b . To single out the strength of non-Gaussian fluctuation from the impact parameter weight at different b , a normalized MSE₀ is used, which reads

$$\text{MSE}_0(P||Q, b) = \frac{1}{S} \sum_{i=1}^S \left(\frac{P(\mathbf{X}_i|b)\Delta b}{2b\Delta b/b_{max}^2} - \frac{Q(\mathbf{X}_i|b)\Delta b}{2b\Delta b/b_{max}^2} \right)^2. \quad (10)$$

The factor $2b\Delta b/b_{max}^2$ comes from the relationship,

$$\int_b^{b+\Delta b} P(\mathbf{X}|b)d\mathbf{X}db \approx 2\pi b\Delta b/\pi b_{max}^2. \quad (11)$$

The MSE₀ as functions of b are plotted in panel (b). When $E_{beam} = 50, 80, 120$ MeV/u, the value of MSE₀ monotonously increase with the impact parameter b . At $E_{beam} = 200$ MeV/u, the values of MSE₀ reach the maximum at $b=9$ fm and then

decreases with impact parameter increase for SkM*. The maximum value of MSE reflects that the strongest nonequilibrium effects, and it could be related to the pseudocritical point in the liquid-gas phase transition for finite systems. Because the long correlation length near the critical point will lead to a non-Gaussian shape of observable distribution. To understand the influence of effective Skyrme interaction on the position of the maximum MSE₀, we also calculate the MSE₀ as a function of b with the parameter set SLy4. Our calculations show that MSE₀ reaches a maximum at $b=9$ fm, which is smaller than that obtained with SkM*. But the difference of MSE₀ obtained with SkM* and SLy4 is small. It implies that the critical temperature for SLy4 and SkM* is different and the difference is small. This trend is consistent with the theoretical predictions[33].

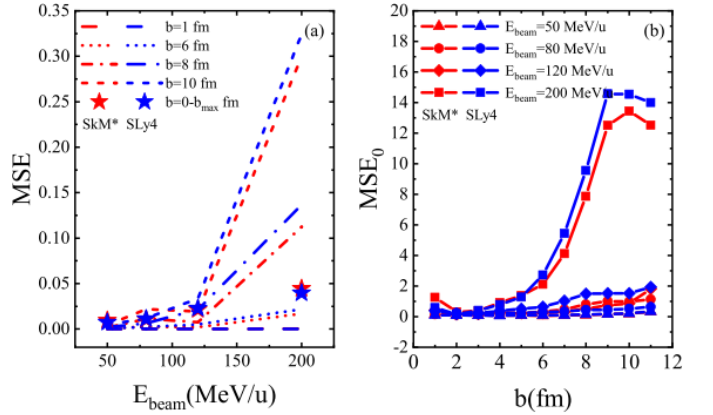


Figure 4: Panel (a) MSE as functions of beam energy. Stars are the results obtained in the whole impact parameter region, and lines are the results for $b=1, 6, 8,$ and 10 fm (lines with different styles); (b) MSE₀ as functions of b at different beam energies .

In summary, the validation of the Bayesian method for reconstructing the impact parameter distribution from the ‘measured’ multiplicity of charged particles and total transverse momentum of light-charged particles under the experimental filters, such as the angle and energy cuts, are tested. Our results show that the experimental conditions do not affect the reliability of the Bayesian method in the reconstruction of impact parameter distribution.

Further, we investigate the deviation of ‘measured’ observables distribution $P(\mathbf{X})$ away from the reconstructed observables distribution $Q(\mathbf{X})$ via the Bayesian method. This deviation reflects the strength of the non-Gaussian fluctuation and can be quantified by the mean-square-error (MSE). Our calculations show that the MSE increases with the beam energy, which is mainly caused by the nonequilibrium dynamics for low-intermediate energy heavy ion collisions. At the beam energy of 200 MeV/u, the non-Gaussian fluctuation reach maximum at $b=9-10$ fm for Sn+Sn, which may be related to the long correlation length and can be used to probe the pseudocritical point for liquid-gas phase transition. It will be exciting to see the experimental results on the MSE, as it can offer valuable insights into nonequilibrium dynamics, and be helpful for estimating the fluctuation caused by high-order correlations and the interplay between geometric symmetry, collective motion,

and stochastic nucleon-nucleon collisions in nuclear collisions.

Acknowledgments

This work was partly inspired by the transport model evaluation project, and it was supported by the National Natural Science Foundation of China under Grants No. 12275359, No. 12375129, No. 11875323 and No. 11961141003, by the National Key R&D Program of China under Grant No. 2023 YFA1606402, by the Continuous Basic Scientific Research Project, by funding of the China Institute of Atomic Energy under Grant No. YZ222407001301, No. YZ232604001601, and by the Leading Innovation Project of the CNNC under Grants No. LC192209000701 and No. LC202309000201. We acknowledge support by the computing server SCATP in China Institute of Atomic Energy.

References

- [1] Wanbing He, Qingfeng Li, Yugang Ma, Zhongming Niu, Junchen Pei, and Yingxun Zhang. Machine learning in nuclear physics at low and intermediate energies. *Science China Physics, Mechanics and Astronomy*, 66:1869, May 2023.
- [2] Scott Pratt, Evan Sangaline, Paul Sorensen, and Hui Wang. Constraining the equation of state of superhadronic matter from heavy-ion collisions. *Phys. Rev. Lett.*, 114:202301, May 2015.
- [3] P. Morfouace, C.Y. Tsang, Y. Zhang, W.G. Lynch, M.B. Tsang, D.D.S. Coupland, M. Youngs, Z. Chajeccki, M.A. Famiano, T.K. Ghosh, G. Jhang, Jenny Lee, H. Liu, A. Sanetullaev, R. Showalter, and J. Winkelbauer. Constraining the symmetry energy with heavy-ion collisions and bayesian analyses. *Physics Letters B*, 799:135045, 2019.
- [4] Wenjie Xie and Bao-An Li. Bayesian inference of the dense-matter equation of state encapsulating a first-order hadron-quark phase transition from observables of canonical neutron stars. *Phys. Rev. C*, 103:035802, Mar 2021.
- [5] Jun Xu, Wenjie Xie, and Bao-An Li. Bayesian inference of nuclear symmetry energy from measured and imagined neutron skin thickness in $^{116,118,120,122,124,130,132}\text{Sn}$, ^{208}Pb , and ^{48}Ca . *Phys. Rev. C*, 102:044316, Oct 2020.
- [6] R. Utama, J. Piekarewicz, and H. B. Prosper. Nuclear mass predictions for the crustal composition of neutron stars: A bayesian neural network approach. *Phys. Rev. C*, 93:014311, Jan 2016.
- [7] Zi-Ao Wang, Junchen Pei, Yue Liu, and Yu Qiang. Bayesian evaluation of incomplete fission yields. *Phys. Rev. Lett.*, 123:122501, Sep 2019.
- [8] Z.M. Niu and H.Z. Liang. Nuclear mass predictions based on bayesian neural network approach with pairing and shell effects. *Physics Letters B*, 778:48–53, 2018.
- [9] Yunfei Ma, Chen Su, Jian Liu, Zhongzhou Ren, Chang Xu, and Yonghao Gao. Predictions of nuclear charge radii and physical interpretations based on the naive bayesian probability classifier. *Phys. Rev. C*, 101:014304, Jan 2020.
- [10] Yifan Liu, Chen Su, Jian Liu, Pawel Danielewicz, Chang Xu, and Zhongzhou Ren. Improved naive bayesian probability classifier in predictions of nuclear mass. *Phys. Rev. C*, 104:014315, Jul 2021.
- [11] Pawel Danielewicz and Mizuki Kurata-Nishimura. Deblurring for nuclei: 3d characteristics of heavy-ion collisions. *Phys. Rev. C*, 105:034608, Mar 2022.
- [12] J. D. Frankland, D. Gruyer, E. Bonnet, B. Borderie, R. Bougault, A. Chbihi, J. E. Ducret, D. Durand, Q. Fable, M. Henri, J. Lemarié, N. Le Neindre, I. Lombardo, O. Lopez, L. Manduci, M. Pärlog, J. Quicray, G. Verde, E. Vient, and M. Vigilante. Model independent reconstruction of impact parameter distributions for intermediate energy heavy ion collisions. *Phys. Rev. C*, 104:034609, Sep 2021.
- [13] Sruthy Jyothi Das, Giuliano Giacalone, Pierre-Amaury Monard, and Jean-Yves Ollitrault. Relating centrality to impact parameter in nucleus-nucleus collisions. *Phys. Rev. C*, 97:014905, Jan 2018.
- [14] Rudolph Rogly, Giuliano Giacalone, and Jean-Yves Ollitrault. Reconstructing the impact parameter of proton-nucleus and nucleus-nucleus collisions. *Phys. Rev. C*, 98:024902, Aug 2018.
- [15] Kianusch Vahid Yousefnia, Atharva Kotibhaskar, Rajeev Bhalerao, and Jean-Yves Ollitrault. Bayesian approach to long-range correlations and multiplicity fluctuations in nucleus-nucleus collisions. *Phys. Rev. C*, 105:014907, Jan 2022.
- [16] Xiang Chen, Li Li, Ying Cui, Junping Yang, Zhuxia Li, and Yingxun Zhang. Bayesian reconstruction of impact parameter distributions from two observables for intermediate energy heavy ion collisions. *Phys. Rev. C*, 108:034613, Sep 2023.
- [17] Kai Wen, Fumihiko Sakata, Zhu-Xia Li, Xi-Zhen Wu, Ying-Xun Zhang, and Shan-Gui Zhou. Non-gaussian fluctuations and non-markovian effects in the nuclear fusion process: Langevin dynamics emerging from quantum molecular dynamics simulations. *Phys. Rev. Lett.*, 111:012501, Jul 2013.
- [18] B. Borderie and J.D. Frankland. Liquid-gas phase transition in nuclei. *Progress in Particle and Nuclear Physics*, 105:82–138, 2019.
- [19] P. Chomaz and F. Gulminelli. Energy correlations as thermodynamical signals for phase transitions in finite systems. *Nucl. Phys. A*, 647:153–171, 1999.
- [20] Philippe Chomaz, Maria Colonna, and Jørgen Randrup. Nuclear spinodal fragmentation. *Physics Reports*, 389(5):263–440, 2004.
- [21] Y. G. Ma, J. B. Natowitz, R. Wada, K. Hagel, J. Wang, T. Keutgen, Z. Maja, M. Murray, L. Qin, P. Smith, R. Alfaro, J. Cibor, M. Cinausero, Y. El Masri, D. Fabris, E. Fioretto, A. Keksis, M. Lunardon, A. Makeev, N. Marie, E. Martin, A. Martinez-Davalos, A. Menchaca-Rocha, G. Nebbia, G. Prete, V. Rizzi, A. Ruangma, D. V. Shetty, G. Souliotis, P. Staszal, M. Veselsky, G. Viesti, E. M. Winchester, and S. J. Yennello. Critical behavior in light nuclear systems: Experimental aspects. *Phys. Rev. C*, 71:054606, May 2005.
- [22] Xin An, Gökçe Başar, Mikhail Stephanov, and Ho-Ung Yee. Non-gaussian fluctuation dynamics in relativistic fluids. *Phys. Rev. C*, 108:034910, Sep 2023.
- [23] T. Pietrzak, A.S. Botvina, J. Brzychczyk, N. Buyukcizmeci, A. Le Fevre, J. Lukasik, P. Pawlowski, C. Sienti, W. Trautmann, and A. Wieloch. The percolation phase transition and statistical multifragmentation in finite systems. *Physics Letters B*, 809:135763, 2020.
- [24] Yingxun Zhang, M.B. Tsang, Zhuxia Li, and Hang Liu. Constraints on nucleon effective mass splitting with heavy ion collisions. *Physics Letters B*, 732:186–190, 2014.
- [25] Ying-Xun Zhang, Ning Wang, Qing-Feng Li, Li Ou, Jun-Long Tian, Min Liu, Kai Zhao, Xi-Zhen Wu, and Zhu-Xia Li. Progress of quantum molecular dynamics model and its applications in heavy ion collisions. *Front. Phys.*, 15:54301, 2020.
- [26] Jun Xu, Lie-Wen Chen, ManYee Betty Tsang, Hermann Wolter, Ying-Xun Zhang, Joerg Aichelin, Maria Colonna, Dan Cozma, Pawel Danielewicz, Zhao-Qing Feng, Arnaud Le Fèvre, Theodoros Gaitanos, Christoph Hartnack, Kyungil Kim, Youngman Kim, Che-Ming Ko, Bao-An Li, Qing-Feng Li, Zhu-Xia Li, Paolo Napolitani, Akira Ono, Massimo Papa, Taesoo Song, Jun Su, Jun-Long Tian, Ning Wang, Yong-Jia Wang, Janus Weil, Wen-Jie Xie, Feng-Shou Zhang, and Guo-Qiang Zhang. Understanding transport simulations of heavy-ion collisions at 100a and 400a mev: Comparison of heavy-ion transport codes under controlled conditions. *Phys. Rev. C*, 93:044609, Apr 2016.
- [27] Hermann Wolter, Maria Colonna, Dan Cozma, Pawel Danielewicz, Che Ming Ko, Rohit Kumar, Akira Ono, ManYee Betty Tsang, Jun Xu, Ying-Xun Zhang, Elena Bratkovskaya, Zhao-Qing Feng, Theodoros Gaitanos, Arnaud Le Fèvre, Natsumi Ikeno, Youngman Kim, Swagata Mallik, Paolo Napolitani, Dmytro Oliinychenko, Tatsuhiko Ogawa, Massimo Papa, Jun Su, Rui Wang, Yong-Jia Wang, Janus Weil, Feng-Shou Zhang, Guo-Qiang Zhang, Zhen Zhang, Joerg Aichelin, Wolfgang Cassing, Lie-Wen Chen, Hui-Gan Cheng, Hannah Elfner, K. Gallmeister, Christoph Hartnack, Shintaro Hashimoto, Sangyong Jeon, Kyungil Kim, Myungkuk Kim, Bao-An Li, Chang-Hwan Lee, Qing-Feng Li, Zhu-Xia Li, Ulrich Mosel, Yasushi Nara, Koji Niita, Akira Ohnishi, Tatsuhiko Sato, Taesoo Song, Agnieszka Sorensen, Ning Wang, and Wen-Jie Xie. Transport model comparison studies of intermediate-energy heavy-ion collisions. *Progress in Particle and Nuclear Physics*, 125:103962, 2022.
- [28] D.G. Sarantites, P.-F. Hua, M. Devlin, L.G. Sobotka, J. Elson, J.T. Hood, D.R. LaFosse, J.E. Sarantites, and M.R. Maier. “the microball” design,

instrumentation and response characteristics of a 4π -multidetector exit channel-selection device for spectroscopic and reaction mechanism studies with gammasphere. *Nuclear Instruments and Methods in Physics Research Section A: Accelerators, Spectrometers, Detectors and Associated Equipment*, 381(2):418–432, 1996.

- [29] F. James and M. Roos. Minuit - a system for function minimization and analysis of the parameter errors and correlations. *Computer Physics Communications*, 10(6):343–367, 1975.
- [30] M. A. Stephanov. Non-gaussian fluctuations near the qcd critical point. *Phys. Rev. Lett.*, 102:032301, Jan 2009.
- [31] Chang Zhou, Ji Xu, Xiaofeng Luo, and Feng Liu. Cumulants of event-by-event net-strangeness distributions in au + au collisions at $\sqrt{s_{NN}} = 7.7$ –200 gev within an urqmd model. *Phys. Rev. C*, 96:014909, Jul 2017.
- [32] Rupam Samanta, João Paulo Picchetti, Matthew Luzum, and Jean-Yves Ollitrault. Non-gaussian transverse momentum fluctuations from impact parameter fluctuations. *Phys. Rev. C*, 108:024908, Aug 2023.
- [33] Arnau Rios. Effective interaction dependence of the liquidus phase transition in symmetric nuclear matter. *Nuclear Physics A*, 845(1):58–87, 2010.